# Materials Horizons



# COMMUNICATION

View Article Online



Cite this: DOI: 10.1039/d4mh00985a

# A transparent p-type semiconductor designed via a polarizability-enhanced strongly correlated insulator oxide matrix†

Received 28th July 2024, Accepted 25th September 2024

DOI: 10.1039/d4mh00985a

rsc.li/materials-horizons

Seung Yong Lee,‡<sup>ab</sup> Inseo Kim,‡<sup>c</sup> Hyun Jae Kim,‡<sup>ad</sup> Sangjun Sim,<sup>c</sup> Jae-Hoon Lee,<sup>ce</sup> Sora Yun,<sup>c</sup> Joonho Bang, <sup>o</sup> Kyoung Won Park, <sup>o</sup> Chul Jong Han,<sup>d</sup> Hyun-Min Kim,<sup>g</sup> Heesun Yang, <sup>o</sup> Bongjae Kim,<sup>h</sup> Seongil Im,<sup>i</sup> Antonio Facchetti, <sup>b</sup> Min Suk Oh, <sup>o</sup> Kyu Hyoung Lee <sup>o</sup> \*<sup>a</sup> and Kimoon Lee <sup>o</sup> \*<sup>ck</sup>

Electron-transporting transparent conducting oxides (TCOs) are a commercial reality, however, hole-transporting counterparts are far more challenging because of limited material design. Here, we propose a strategy for enhancing the hole conductivity without deteriorating the band gap  $(E_{\alpha})$  and workfunction  $(\Phi)$  by Cu incorporation in a strongly correlated NiWO<sub>4</sub> insulator. The optimal Cudoped NiWO<sub>4</sub> (Cu<sub>0.185</sub>Ni<sub>0.815</sub>WO<sub>4</sub>) exhibits a resistivity reduction of  $\sim 10^9$  times versus NiWO<sub>4</sub> as well as band-like charge transport with the hole mobility approaching 7 cm<sup>2</sup> V<sup>-1</sup> s<sup>-1</sup> at 200 K, a deep  $\Phi$ of 5.77 eV, and  $E_{\alpha}$  of 2.8 eV. Experimental and theoretical data reveal that the strength of the electron correlation in NiWO<sub>4</sub> is unaffected by Cu incorporation, while the promoted polarizability weakens electron-phonon coupling, promoting the formation of large polarons. Quantum dot light-emitting and oxide p/n junction devices incorporating Cu<sub>0.185</sub>Ni<sub>0.815</sub>WO<sub>4</sub> exhibit remarkable performances, demonstrating that our approach can be deployed to discover new p-type TCOs.

#### New concepts

In the present work, we report a novel strategy for developing an outstanding transparent p-type (semi)conducting oxide (p-TCO), exhibiting the deepest work function as well as a wide band gap in comparison to other p-TCOs to date, by engineering the polarizability of a strongly correlated oxide matrix through a conventional chemical route of atomic substitution. By substituting Cu into strongly correlated NiWO4, we successfully achieve the composition  $Cu_{0.185}Ni_{0.815}WO_4$  with a high hole carrier mobility approaching 7 cm2 V-1 s-1 at 200 K, a deep work function of 5.77 eV, and a large optical gap  $E_{\rm g}$  of 2.8 eV (even 3.8 eV in direct  $E_g$ ). Equally important, this new oxide material composition exhibits a band-like large polaronic conduction achieved without disturbing the Ni d-d electron correlation strength, which is associated with the deepest-lying delocalized valence band maximum state in metal oxides, to the best of our knowledge. As a practical application, we also demonstrate that the best composition functions as an efficient hole transporting layer in a quantum dot light-emitting diode as well as an oxide p/n junction rectifier, enabling high luminescence/efficiency and on/off switching ratio, respectively.

## Introduction

Several modern (opto)electronic devices utilize the complementary charge transport in semiconductors for optimal operation. <sup>1-8</sup> Manipulating their conduction and transition with opposite polarities at a distinct energetic potential has been a great

technological issue covering systems ranging from traditional Si-based circuitries to nanoscale systems beyond the quantum limit.<sup>1–8</sup> For instance, complementary metal-oxide-semiconductor-type (CMOS-type) electronic devices operate by simultaneous opposite switching behaviour based on rationally connected n-

a Department of Materials Science and Engineering, Yonsei University, Seoul 03722, Republic of Korea. E-mail: khlee2018@yonsei.ac.kr

<sup>&</sup>lt;sup>b</sup> KIURI Institute, Yonsei University, Seoul 03722, Republic of Korea

<sup>&</sup>lt;sup>c</sup> Department of Physics, Kunsan National University, Gunsan 54150, Republic of Korea. E-mail: kimoon.lee@kunsan.ac.kr

<sup>&</sup>lt;sup>d</sup> Display Research Center, Korea Electronics Technology Institute (KETI), Seongnam 13509, Republic of Korea. E-mail: ohms@keti.re.kr

<sup>&</sup>lt;sup>e</sup> Global Infra Technology, Samsung Electronics, Yongin 17113, Republic of Korea

f School of Materials Science & Engineering, Gyeongsang National University, Jinju 52828, Republic of Korea

g Department of Materials Science and Engineering, Hongik University, Seoul 04066, Republic of Korea

<sup>&</sup>lt;sup>h</sup> Department of Physics, Kyungbuk National University, Daegu 41566, Republic of Korea

<sup>&</sup>lt;sup>i</sup> Department of Physics, van der Waals Materials Research Center, Yonsei University, Seoul 03722, Republic of Korea

<sup>&</sup>lt;sup>j</sup> School of Materials Science and Engineering, Georgia Institute of Technology, Atlanta, GA 30332, USA. E-mail: afacchetti6@gatech.edu

<sup>&</sup>lt;sup>k</sup> The Institute of Basic Science, Kunsan National University, Gunsan 54150, Republic of Korea

<sup>†</sup> Electronic supplementary information (ESI) available. See DOI: https://doi.org/10.1039/d4mh00985a

<sup>‡</sup> These authors contributed equally to this work.

Communication **Materials Horizons** 

and p-type transistors in which electrons and holes serve as the majority current deliverer, respectively.<sup>1-3</sup> Optoelectronic devices, such as photodetectors/emitters and photovoltaic cells, also employ excitation/recombination processes between electrons and holes lying at distant energy levels. 5-8 Transparent conducting oxides (TCOs) are (semi)conductors that are transparent in the visible spectrum and can transport both electrons and holes, with the former widely commercialized.<sup>3,8-14</sup> In particular, their optical transparency and large exciton binding energy even over large electrical conductivity ( $\sigma$ ) variations have paved the way for several applications from defrosting to ultra-high definition (UHD) displays and smart functional windows.3,8-13 Despite such advances, improvements of TCO-based devices remain hindered by the imbalanced performance between n- and p-type TCOs, thus a strategy to balance their transport is critical to realize new types of devices.3,9,14

The main obstacle inhibiting charge transport balance in TCOs is the trade-off relationship between hole carrier mobility  $(\mu_{\rm H})$  and the optical band gap  $(E_{\rm g})$ . <sup>8-11,14</sup> Because a deep-lying valence band maximum (VBM) state across a large  $E_g$  typically results in a narrow bandwidth/poor orbital overlap and localized hole transport when approaching core levels, 8-11,14-18 the realization of p-type TCOs exhibiting respectable  $\mu_{\rm H}$ , wide  $E_{\rm g}$ , as well as deep work function  $(\Phi)$  is far more challenging than for n-type ones. In addition, the optical transparency critically relates to  $E_{\rm g}$  that could be narrowed with elevating VBM level position, and deep  $\Phi$  is favoured to secure wide  $E_{\rm g}$ . To overcome this limitation, several studies have explored Cu- or Sn-based oxides whose VBM partially comprises more diffused metal d and/or s-orbitals.3,9,14,15 However, because of the raised VBM energy, these materials exhibit an  $E_{\rm g}$  value and a  $\Phi$  value smaller than  $\sim 2$  and  $\sim 5$  eV, respectively, thus they are poorly transparent and inefficient for hole injection/extraction. 3,9,14,15 Recent studies suggest that strongly correlated metallic oxides could be a new entry for p-type TCO candidates. 19,20 From the large effective mass under strong electron-electron interactions, the free carrier reflection edge shifts outside the visible energy range, thus visible transparency can be attained even under high hole carrier concentrations greater than  $\sim 10^{21}$  cm<sup>-3</sup>. <sup>19,20</sup> However, this metallic nature inherently leads to a high absorption coefficient and screens the electric field in field-effect transistor (FET) devices, therefore only very thin layers (<10 nm) can be utilized to secure optical transparency and prevent their use as FET-active channel layers. 19,20

Recently, we proposed a compositional tuning approach for enhancing hole conductivity while maintaining a wide band gap  $(E_g)$  by utilizing a Mott-Hubbard insulator system with strong electron correlation.<sup>21</sup> By partial substitution of Ni with Cu in NiO, the polaron hopping efficiency was improved without much suppression of the correlation strength. However, this material showed a very low  $\mu_{\rm H}$  of 0.007 cm<sup>2</sup> V<sup>-1</sup> s<sup>-1</sup>, and the charge transport remains dominated by the small polaron hopping (SPH) limit. Inspired by the previous study, we hypothesized that a less correlated system, possibly alleviating polaronic distortion, could lead to greater hole mobility and band-like charge transport while retaining a deep-lying VBM

and transparency. In this study, we report ternary (monoclinic) NiWO<sub>4</sub> with lower symmetry than binary (cubic) NiO as the matrix material to prove this concept. By synthesizing Cusubstituted NiWO<sub>4</sub> (Ni<sub>1-x</sub>Cu<sub>x</sub>WO<sub>4</sub>, 0.00  $\leq x \leq$  0.20), a considerable increase in the electrical conductivity by  $\sim 10^9$  times for x = 0.20, compared to that of intrinsic NiWO<sub>4</sub>, was measured. From electrical, optical, magnetic, and theoretical characterization, Cu substitution in NiWO<sub>4</sub> gives rise to high  $\mu_H$ approaching 7 cm<sup>2</sup> V<sup>-1</sup> s<sup>-1</sup> at 200 K, exhibiting nonthermally activated behaviour without much variation both in  $E_{\sigma}$  and the magnetic transition temperature. This result demonstrates the emergence of large polaronic hole conduction under a sustained correlation strength. The excellent  $E_{\sigma}$  and  $\Phi$  values larger than 2.7 and 5.56 eV, respectively, even at a high Cu content of 0.20 demonstrate that such delocalized hole conduction occurs through a very deep-lying VBM and a wide  $E_g$ , which is essential for optimal p-type TCO. This newly developed Ni<sub>1-x</sub>Cu<sub>x</sub>WO<sub>4</sub> functions as an efficient hole transporting layer (HTL) in both quantum dot light-emitting diodes (QD-LEDs) and oxide-based p/n junction rectifiers, further corroborating the potential of this p-type TCO for practical applications.

# Methods

#### Materials synthesis and characterization

Polycrystalline Ni<sub>1-x</sub>Cu<sub>x</sub>WO<sub>4</sub> were synthesized by a solid-state reaction process. After mixing stoichiometric amounts of NiO, CuO, and WO<sub>3</sub> powders (99.998%, 99.995% and 99.998% purity, respectively) in an agate mortar, these mixtures were annealed at 950 °C for 24 h. The annealed powders were pulverized, then pressed into a pellet form, followed by heating at 950 °C for 24 h. By repeating the same pulverizing/pressing and annealing processes two more times, homogeneous and single phase  $Ni_{1-x}Cu_xWO_4$  samples  $(0.00 \le x \le 0.20)$  could be finally obtained. The crystalline structures of the synthesized samples were analysed by XRD measurement (MiniFlex 600, Rigaku). Compositional analysis was performed by inductively coupled plasma mass spectroscopy (ICP-MS) (7900 ICP-MS, Agilent). The vibrational modes of the Ni<sub>1-x</sub>Cu<sub>x</sub>WO<sub>4</sub> samples were characterized by Raman spectroscopy with 532 nm wavelength excitation (RAMANtouch, nanophoton). The electrical resistivity in the high T region (300-570 K) was measured by a 4-point-probe method using a semiconductor parameter analyser (4200-SCS, Keithley). Hall-effect measurements in the low T region (160-260 K) were carried out by utilizing a high-precision current source, nanovolt meter, and Hall-effect card (6220, 2182A, and 3756, Keithley, respectively) equipped with a cryogen-free cryostat and a 1.2 T electro-magnet. (Co-designed by I.V SOLUTION and Sungwoo Instruments Inc.) For the electrical measurement, we applied Ag paste on the square-cutting densified pellet (the inset photo in Fig. 1c) with Hall-bar geometry, then wired it to the external instruments. Optical absorption spectra and magnetic properties were investigated by a spectroscopic ellipsometer (M-2000, JA Woollam) and magnetic property measurement system (MPMS, Quantum Design), respectively. Ultraviolet photoemission spectroscopy (UPS)

Materials Horizons Communication

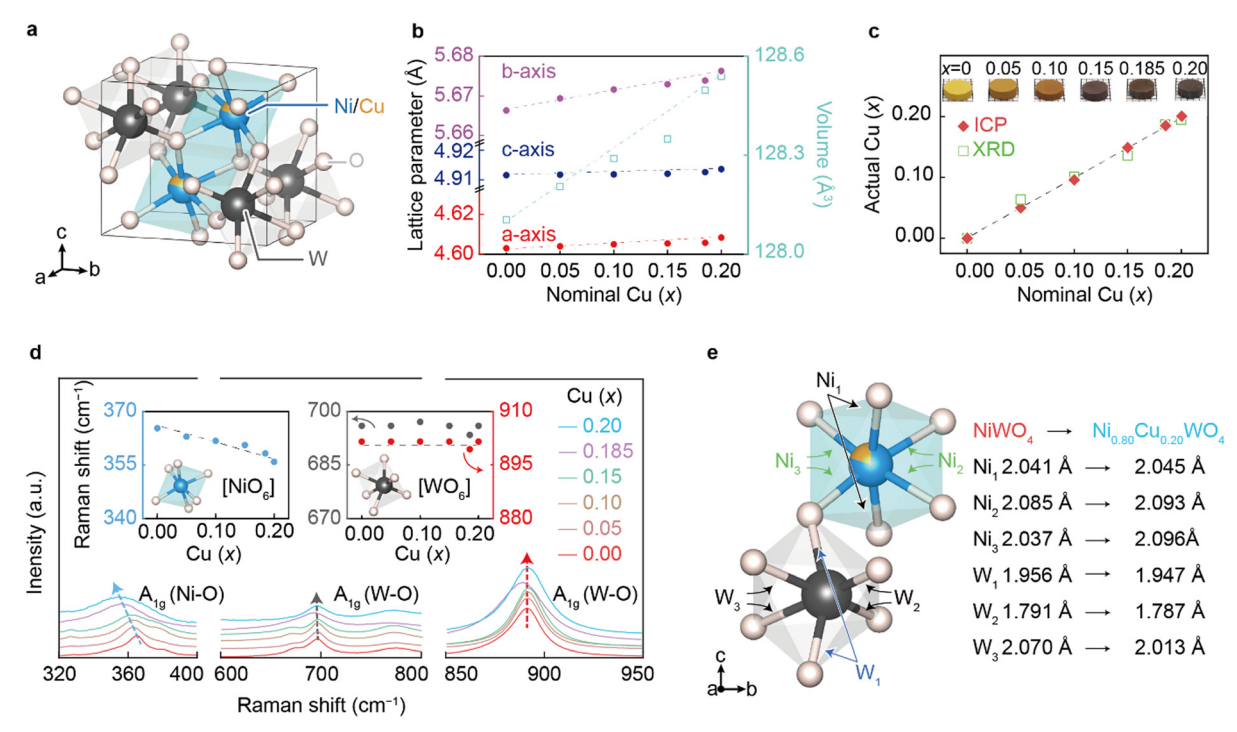


Fig. 1 Characterization of  $Ni_{1-x}Cu_xWO_4$  samples. (a) Crystal structure of  $Ni_{1-x}Cu_xWO_4$  (0.00  $\leq x \leq$  0.20) obtained by the Rietveld refinement of PXRD patterns. (b) Lattice parameters and unit cell volume from PXRD data as a function of x. (c) Atomic composition of Cu-substitution contents, x, characterized by ICP-MS and Rietveld analysis. The inset photo displays the colours of synthesized  $Ni_{1-x}Cu_xWO_4$  samples with different x values. (d) Raman spectra from  $Ni_{1-x}Cu_xWO_4$  samples. The characteristic peak positions for Ni-O and W-O vibrational modes as a function of x are plotted in the inset. (e) The local structure of  $[NiO_6]$  and the nearest  $[WO_6]$  octahedral units. The bond length changes with Cu substitution are also defined.

measurements were carried out by using a hemispherical analyser with a He I (21.2 eV) source (AXIS Supra $^+$ , KRATOS Analytical). For insulating the surface nature of Ni $_{1-x}$ Cu $_x$ WO $_4$ , the charge neutralization system was applied onto the ion-etched surface under a sample bias of -10 V to obtain the true cut-off of the secondary electron emission. Electrical permittivity was measured by an impedance analyser (HP4284, Agilent) with varying frequency from 1 kHz to 1 MHz at 300 K.

#### Density functional theory (DFT) calculations

All DFT calculations were performed using the projector augmented wave (PAW) method implemented in the Vienna ab initio simulation package (VASP) code. 22,23 Starting from the experimental input, the lattice parameters and internal coordinates of the atoms were fully relaxed with a force criteria of 1 meV Å<sup>-1</sup>. We employed the generalized gradient approximation (GGA) exchange-correlation potential with a plane-wave energy cut-off of 500 eV.24 It was confirmed that the magnetic ground state was well reproduced by total energy calculation (see Fig. S1, ESI†). To study the substitution effect, a twice larger supercell was constructed, which includes 8 f.u. and one Ni out of eight was substituted with Cu to simulate the x = 0.125substitution case.  $4 \times 8 \times 8$  and  $4 \times 8 \times 4$  of k-point meshes were sampled for pristine and Cu-substituted NiWO<sub>4</sub>, respectively. To treat the correlation of transition metal d-electrons, U = 6 eV and 8 eV were used for Ni 3d and Cu 3d with a Dudarev scheme within the DFT+U approach. 25-27

#### **OD-LED** device fabrication and characterization

To fabricate QD-LED devices, indium tin oxide (ITO, 150 nm) coated glass substrates (25  $\times$  25 mm<sup>2</sup>) were patterned by the conventional photolithography method and wet etching process after cleaning with acetone, methanol, and isopropyl alcohol (IPA) by ultrasonic cleaner. Then the substrates were rinsed with deionized water and blown with N2. The patterned ITO glass substrates were treated by O2 plasma at 150 W for 300 s, then 1.25 wt% tungsten oxide nanoparticles (~30 nm, Sigma-Aldrich) in 2-propanol were spin-coated onto the ITO glasses at 500 rpm for 5 s and 5500 rpm for 30 s. To remove the residual solvent, they were baked at 100 °C for 30 min. The 30 nm-thick Ni<sub>0.815</sub>Cu<sub>0.185</sub>WO<sub>4</sub> layers as the hole transport layer (HTL) were deposited by an RF magnetron sputtering process (10 mTorr, 100 W) using a sintered target with the same stoichiometry through a shadow mask in ambient Ar at RT, (deposition rate was 8.3 nm min<sup>-1</sup>) followed by a rapid thermal annealing process at 300  $^{\circ}$ C for 10 min in ambient O<sub>2</sub> (3  $\times$  $10^2$  Torr). As the emission layer, CdSe-based QDs of 10 mg mL<sup>-1</sup> in toluene were spin-coated on the Ni<sub>0.815</sub>Cu<sub>0.185</sub>WO<sub>4</sub>-deposited substrates at 500 rpm for 2 s and 2000 rpm for 20 s (details of the synthetic process for the QDs are described in the ESI†). After QD coating, the substrates were treated at 100 °C for 10 min on a hot plate in the glove box. As the electron transport layer (ETL) and electron injection layer (EIL), we deposited TPBi (1,3,5-tris(1phenyl-1H-benzimidazol-2-yl)benzene, Luminescence Technology Corp.) and lithium fluoride (LiF), respectively, by thermal

**Materials Horizons** Communication

evaporation. For the cathode, 80 nm-thick Al was deposited through a shadow mask by thermal evaporation. The fabricated devices were encapsulated by the encapsulation glass using UV sealant in the glove box with nitrogen. The device structure was measured by HR-TEM (JEM-2100F, JEOL). The current density-voltage-luminance (I-V-L) characteristics and electroluminescence (EL) spectra of QD-LEDs were measured by a spectroradiometer (CS-2000A, Konica Minolta) and Keithley 2400 Source Measure Unit.

## Oxide p/n junction rectifying device fabrication and characterization

To fabricate p-Ni<sub>0.815</sub>Cu<sub>0.185</sub>WO<sub>4</sub>/n-IGZO junction rectifying device, indium tin oxide (ITO, 150 nm) coated glass substrates  $(25 \times 25 \text{ mm}^2)$  were cleaned with acetone, methanol, and isopropyl alcohol (IPA) by ultrasonic cleaner. Then the substrates were rinsed with deionized water and blown with N2. The 100 nm-thick IGZO film was RF sputtered onto the cleaned ITO glasses (3 mTorr, 100 W) under working pressure of Ar/O<sub>2</sub>  $(Ar: O_2 = 10:1)$  conditions (deposition rate was 1.4 nm min<sup>-1</sup>), followed by a rapid thermal annealing process at 300 °C for 10 min in ambient air. The same 100 nm-thick  $Ni_{0.815}Cu_{0.185}WO_4$ layer was also deposited by an RF magnetron sputtering process (10 mTorr, 100 W) using the same sintered target with a HTL in QD-LED in  $Ar: O_2 = 2:1$  ambient at RT, followed by a rapid thermal annealing process at 300 °C for 10 min in ambient O2  $(3 \times 10^2 \text{ Torr})$ . For the top-contact ohmic electrode, 100 nmthick Au was deposited through a shadow mask by thermal evaporation. Static current-voltage (I-V) characteristics were measured using a semiconductor parameter analyzer (4200-SCS, Keithley) under dark and ambient air conditions at RT. The dynamic rectifying characteristics of a fabricated p-Ni<sub>0.815</sub>-Cu<sub>0.185</sub>WO<sub>4</sub>/n-IGZO junction rectifier under various AC conditions were measured using a function generator (AFG 3022B, Tektronix) and an oscilloscope (TDS 2014B, Tektronix) with a serial  $R_{\rm L}$  of 100 k $\Omega$  at RT.

# Results & discussion

#### Materials synthesis and characterization

For sample preparation, we synthesized Ni<sub>1-x</sub>Cu<sub>x</sub>WO<sub>4</sub> with different x contents from 0 to 0.25 through the conventional solid-state reaction process (see details in the Methods section). Fig. 1a illustrates the crystal structure of Ni<sub>1-x</sub>Cu<sub>x</sub>WO<sub>4</sub> for different x values obtained by Rietveld refinement of the powder X-ray diffraction (PXRD) measurements (see Fig. S2, S3 and Table S1 for details, ESI†). Regardless of the x value, all samples show a monoclinic structure with a space group of P12/c1, belonging to a relatively low symmetry group compared to cubic binary NiO.21 PXRD shows no observable impurity except for the sample with x = 0.25, as marked by the asterisk in Fig. S2 (ESI†). As shown in Fig. 1b, the unit cell volume linearly increases with increasing x, mainly originating from the b-axis expansion. Accompanied by the quantitative x values plotted in Fig. 1c (Table S2, ESI†), this result demonstrates that Cu

homogeneously substitutes Ni forming a solid solution, data consistent with the Rietveld refinement results and the Vegard's rule.21 Fig. 1d shows the Raman spectra in selected regions for Ni<sub>1-x</sub>Cu<sub>x</sub>WO<sub>4</sub> samples (for full-range spectra see Fig. S4, ESI†). The Raman peak at  $\sim 370 \text{ cm}^{-1}$  originates from symmetric A<sub>1g</sub> vibration of [NiO<sub>6</sub>] octahedra, while those at  $\sim 700$  and  $\sim 900$  cm<sup>-1</sup> are assigned as W-O-W and [WO<sub>6</sub>] octahedra symmetric vibration modes, respectively<sup>28</sup> (see Fig. 1d). Note that the vibrational energy is proportional to  $\sqrt{k/\mu}$ , where k and  $\mu$  are the spring constant and the reduced mass, respectively, resulting in the systematic Raman peak shift associated not only to the change of  $\mu$  but also to the strain effect in the substitutional solid-solution system.<sup>29</sup> Since the Raman peak associated with [NiO<sub>6</sub>] octahedra redshifts with increasing x, in contrast to the negligible changes in the  $[WO_6]$ associated peaks, this result further demonstrates that Cu substitutes Ni and not W as evidenced by the bond length changes depicted in the local structure of corner-sharing [NiO<sub>6</sub>] and its neighbouring [WO6] (Fig. 1e). Element mapping by scanning electron microscopy (SEM) - energy dispersive X-ray spectroscopy (EDS) also confirms that Cu-substitutions are uniformly distributed through the whole sample area (see Fig. S5, ESI†).

#### Charge carrier transport analysis

The electrical properties of the Ni<sub>1-x</sub>Cu<sub>x</sub>WO<sub>4</sub> samples were measured using densified pellet forms in contact with Ag paste electrodes with Hall bar geometry (details in the Methods section). Fig. 2a displays the changes in the electrical resistivity  $(\rho)$  at 300 K for Ni<sub>1-x</sub>Cu<sub>x</sub>WO<sub>4</sub> samples, demonstrating that  $\rho$ drastically decreases from  $3.69 \times 10^{12}$  to  $3.28 \times 10^{3}$   $\Omega$ ·cm as x increases. When we measured the temperature (T) dependence of  $\rho$  from 300 to 570 K, we found that all samples show thermally activated behaviour regardless of x, as shown in Fig. 2b. Note that a kink at  $\sim 400$  K for x = 0 is possibly due to the mixed conduction at high T,30 however, all samples display a linear relationship in the  $ln(\rho/T)$  versus 1/T plot. This demonstrates that the charge transport mechanism in  $Ni_{1-x}Cu_xWO_4$  at high T (where the electron-phonon interaction is strong) follows the SPH model, resulting in relatively low  $\mu_{
m H}$  values in line with other Ni-based transition metal oxides. 17,18,20,21 However, the slope of the  $\ln(\rho/T)$  versus 1/Tplot decreases as x increases (Fig. 2a), confirming that the activation energy  $(E_a)$  for SPH conduction is suppressed upon Cu incorporation as also observed in Cu-substituted NiO. Note that the smallest  $E_a$  corresponds to a value of 0.16 eV versus 0.24 eV measured for NiO,21 suggesting that the hopping probability in monoclinic ternary NiWO4 is much improved compared to that in the rigid cubic binary NiO system.

To investigate charge transport details in Ni<sub>1-x</sub>Cu<sub>x</sub>WO<sub>4</sub>, we performed Hall-effect measurements on the most conductive samples with x = 0.185 and 0.20 at low T(160-260 K), where the phonon-associated interaction is relatively inactive. 17,18,31 Fig. 2c-e report  $\sigma$ , the carrier concentration (p), and  $\mu_{\rm H}$ as a function of T. From Fig. 2c, both samples show similar

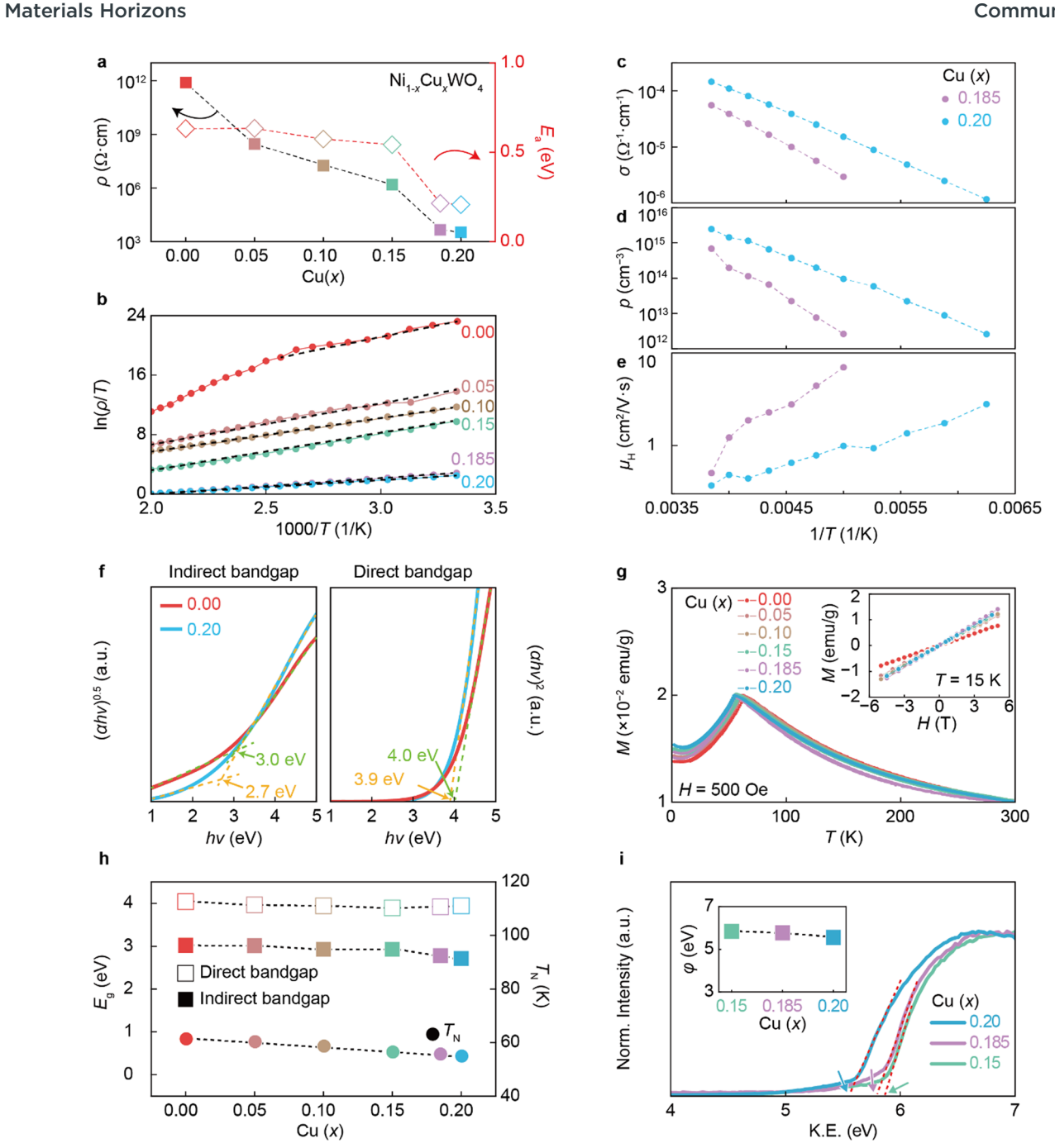


Fig. 2 Physical properties of the  $Ni_{1-x}Cu_xWO_4$  samples. (a) Changes of  $\rho$  and activation energy for small polaron hopping as a function of x in  $Ni_{1-x}Cu_xWO_4$ . (b)  $In(\rho/T)$  versus 1/T curves from 300 to 570 K for various x. The linear slopes for estimating activation energy are marked by dashed lines. The 1/T dependence of (c)  $\sigma$ , (d) p, and (e)  $\mu_H$  for Ni<sub>1-x</sub>Cu<sub>x</sub>WO<sub>4</sub> with x = 0.185 and 0.20 in the low T region (160–260 K). (f) Indirect and direct  $E_q$ estimation for  $Ni_{1-x}Cu_xWO_4$  samples with x=0.00 and x=0.20 by fitting optical absorption spectra. (g) M versus T curves measured under H of 500 Oe. M versus H curves measured at 15 K are also shown in the inset. (h)  $E_0$  and  $T_N$  values with respect to x in  $Ni_{1-x}Cu_xWO_4$ . (i) Cut-off energy obtained by UPS spectra from secondary electron emission for  $Ni_{1-x}Cu_xWO_4$  samples with x = 0.15, 0.185, and 0.20. The inset shows the extracted  $\Phi$  values with respect to x.

thermally activated behaviour of  $\sigma$  in the high T region. In contrast to the high T region, definite Hall voltages with positive values start to be detected in the low T region for x = 10.185 and 0.20, revealing the p-type polarity of Ni<sub>1-x</sub>Cu<sub>x</sub>WO<sub>4</sub>. Based on the measured Hall voltage with decreasing T, we can obtain a  $\log p$  versus 1/T plot as shown in Fig. 2d. When we

extracted the acceptor ionization energy by extrapolating the Arrhenius relationship, values of 0.68 and 0.52 eV are obtained for x = 0.185 and 0.20, respectively, indicating the quite far energetic distance between the acceptor level and the VBM for hole carrier generation. From the relationship  $\sigma = p \cdot e \cdot \mu_H$ , where e is the elemental charge, the T dependence of  $\mu_{\rm H}$  can be

Communication **Materials Horizons** 

plotted as displayed in Fig. 2e. Note that  $\mu_{\rm H}$  increases, reaching the highest value of 6.98 cm<sup>2</sup> V<sup>-1</sup> s<sup>-1</sup> (at 200 K for x = 0.185), with decreasing T, overcoming the thermally activated behaviour of both samples. This result strongly evidences the emergence of band-like transport dominated by electron-phonon interactions distinctly different from hopping conduction, 17,18,31 suggesting that Cu substitution in NiWO<sub>4</sub> plays a critical role as an  $\mu_{\rm H}$ enhancer rather than an acceptor impurity.

#### Degree of electron correlation related with band energy level

Fig. 2f shows the optical absorption spectra for indirect and direct  $E_g$  estimation from  $Ni_{1-x}Cu_xWO_4$  samples with x = 0.00and 0.20. The spectra for other compositions are displayed in Fig. S6 (ESI†). As shown in Fig. 2f, an indirect transition of 3.0 eV occurs in NiWO<sub>4</sub> (x = 0.00), while a slightly suppressed transition of 2.7 eV with x = 0.20 is measured from the  $(\alpha h v)^{0.5}$ plot, where  $\alpha$  and hv denote the absorption coefficient and incident optical energy, respectively. Both samples exhibit direct transition values of approximately 4.0 eV as plotted in Fig. 2f. This result is consistent with the Cu-substituted NiO case, supporting that the electron correlation strength, which is expected to be the main origin for  $E_{\rm g}$  formation, remains unaffected, resulting in an almost constant  $E_{\rm g}$  value even for a high Cu content of 0.20.21 This degree of correlation could also be estimated from the magnetic properties. Fig. 2g shows the Tdependence of the magnetization (M) for Ni<sub>1-r</sub>Cu<sub>r</sub>WO<sub>4</sub> samples. Antiferromagnetic (AFM) ordering occurs near 61 K for intrinsic NiWO<sub>4</sub>, which is consistent with previous reports.<sup>32</sup> When Cu is introduced, the Néel temperature  $(T_N)$  does not change much, with a slight decrease to 55 K even for a high x Cu concentration of 0.20. This result shows that the magnetism of the system is mostly governed by Ni. Together with the result that the magnetic field (H)-dependent M for all the samples shows a linear relationship without any hysteresis (Fig. 2ginset), the AFM ground states are not changed by introducing Cu.<sup>21</sup> Importantly,  $E_{\rm g}$  and  $T_{\rm N}$  do not change up to a x=0.20 (Fig. 2h). Assuming a strongly correlated nature of NiWO<sub>4</sub> similar to that of AFM NiO, both  $T_{\rm N}$  and  $E_{\rm g}$  critically depend on the exchangecorrelation strength, i.e. U/t, where U is the Coulomb potential, and t is the transfer integral between Ni 3d electrons. 33 This result strongly suggests that the strength of the electron correlation in NiWO<sub>4</sub> is not affected by Cu substitution.

To understand whether this kind of rigid correlation also operates at the energy band level, UPS measurements were carried out and a comprehensive band schematic is displayed in Fig. S7 (ESI†). As shown in Fig. 2i, the  $\Phi$  values can be defined by the cut-off energy of the secondary electron emission obtained from the polycrystalline Ni<sub>1-x</sub>Cu<sub>x</sub>WO<sub>4</sub> surfaces with x = 0.15, 0.185, and 0.2. Plotting  $\Phi$  with respect to x(Fig. 2i-inset) indicates that  $\Phi$  is not very suppressed when varying x, data consistent with the  $E_{\rm g}$  and  $T_{\rm N}$  results. Valence band spectra for all measured samples show states that disappear close to the Fermi level ( $E_{\rm F}$ , see Fig. S8, ESI†), indicating almost identical  $\Phi$  to the VBM level as a representative feature from the strongly correlated oxide with partially occupied d-bands with a high number of electrons. 15 This result strongly

supports that the VBM band energy level in p-type NiWO4 is pinned, and remains deeper than 5.56 eV associated with the rigid correlation strength with Cu substitution, while retaining the  $\mu_{\rm H}$  of other p-TCOs (Table S3, ESI†).

#### Theoretical confirmation of a strongly correlated behaviour

To elucidate the underlying physics of the unprecedented charge transport behaviour, we performed DFT calculations. The band structures of the intrinsic NiWO<sub>4</sub> and Ni<sub>1-x</sub>Cu<sub>x</sub>WO<sub>4</sub> (x = 0.125) are shown in Fig. 3a-d. Expectedly, without the explicit consideration of the electronic correlation in Ni d orbitals,  $E_{\rm or}$  is considerably underestimated ( $\sim 0.83$  eV). With the direct inclusion of the Ni d Hubbard  $U(U_{Ni})$  of 6 eV, in the form of DFT+U, the gap increases and becomes comparable to the experimental value of 3.0 eV. Compared to other systems with a p-d gap, where the Hubbard U does not contribute to the size of the gap, here it evidences the strong d-d character of the gap. 33,35 For the Cu-substituted case, to account for the higher occupation of Cu d-orbitals, we employed a Hubbard  $U(U_{Cu})$  of 8 eV for Cu d,25-27 which is slightly larger than the corresponding value for Ni. In between the d-d gap originating from Ni, the Cu d state is formed, which in turn slightly decreases the size of the  $E_{\rm g}$ . This behaviour is consistent with the experimental optical absorption results in Fig. 2h. Our calculations show the importance of explicit inclusion of the Coulomb U in partially filled d-orbital systems, and unambiguously demonstrates the strongly correlated nature of the newly developed Ni<sub>1-x</sub>Cu<sub>x</sub>WO<sub>4</sub> p-type semiconductors. Fig. 3e-h display the corresponding partial density of states (PDOS) of NiWO<sub>4</sub> and  $Ni_{1-x}Cu_xWO_4$  (x = 0.125). We can clearly observe the shift of the Ni and Cu d orbitals upon the inclusion of U. Fig. S9 and S10 (ESI†) report the systematic evolution of the PDOS upon the inclusion of  $U_{Ni}$  and  $U_{Cu}$ , respectively. The PDOSs also confirm that the correlated electrons of localized d orbitals from Ni and Cu govern the low-energy physics of the system, and are the main origin for the almost invariant  $E_{\rm g}$  and deep  $\Phi$  value insensitive to the Cu impurity substitution concentration.

## Polarizability estimation analysis related to large polaronic conduction

Fig. 3i and j show the calculated charge density map near the VBM from  $E_F$  - 1 eV to  $E_F$  for NiWO<sub>4</sub> and Ni<sub>0.875</sub>Cu<sub>0.125</sub>WO<sub>4</sub>, respectively. Thus, by replacing Ni with Cu the charge distribution changes both at the transition metal and the O sites. By comparing the PDOSs for the pristine and Cu-substituted cases in Fig. 3f and h, respectively, the hybridization of O p states, especially near the  $E_{\rm F}$ , is enhanced, which is reflected in the charge density plot in Fig. 3i and j. This data, in turn, affects the overall polarizability of the system. This enhanced polarizability can be experimentally monitored by measuring the electrical permittivity ( $\varepsilon$ ) (Fig. 3k). From impedance spectroscopy measurements,  $\varepsilon$  increases under a wide frequency regime from 1 kHz to 1 MHz upon increasing the Cu content from 0.00 to 0.20 (the possible origins for the increment on  $\varepsilon$ are discussed in Section S12 in the ESI†). The dimensionless electron-phonon coupling constant ( $\alpha$ ) is given by the following

NiWO, NiWO,  $Ni_{0.875}Cu_{0.125}WO_{4}$  $Ni_{0.875}Cu_{0.125}WO_{4}$ (U, =0 eV) (U<sub>Ni</sub>=6 eV) (U<sub>Ni</sub>=6 eV, U<sub>CII</sub>=0 eV) (U<sub>Ni</sub>=6 eV, U<sub>CII</sub>=8 eV) Energy (eV) Spin up 2.57 eV 2.57 eV Spin down AX H1IM D ZIY AX H1IM D ZIY HEAXHIIM DZIY Total - W - Total - W-d DOS (states/eV) - Ni-d O-n 2.54 eV 2.57 eV Cu-d 2 Energy (eV) Energy (eV) Energy (eV) Energy (eV) NiWO,  $Ni_{0.875}Cu_{0.125}WO_{4}$ k Cu (x) • 0 00 • 0 15 0.05 --- 0.185 0.10 - 0.2010 ω 10° 10

Fig. 3 Electron correlation and polarizability study in NiWO<sub>4</sub> and Ni<sub>1-x</sub>Cu<sub>x</sub>WO<sub>4</sub>. Band dispersion calculated from (a) NiWO<sub>4</sub> ( $U_{Ni}=0$  eV), (b) NiWO<sub>4</sub> ( $U_{Ni}=6$  eV), (c) Ni<sub>0.875</sub>Cu<sub>0.125</sub>WO<sub>4</sub> ( $U_{Ni}=6$  eV),  $U_{Cu}=0$  eV), and (d) Ni<sub>0.875</sub>Cu<sub>0.125</sub>WO<sub>4</sub> ( $U_{Ni}=6$  eV). The respective total/projected DOS of Ni, W, Cu, and O obtained from (e) NiWO<sub>4</sub> ( $U_{Ni}=0$  eV), (f) NiWO<sub>4</sub> ( $U_{Ni}=6$  eV), (g) Ni<sub>0.875</sub>Cu<sub>0.125</sub>WO<sub>4</sub> ( $U_{Ni}=6$  eV),  $U_{Cu}=0$  eV), and (h) Ni<sub>0.875</sub>Cu<sub>0.125</sub>WO<sub>4</sub> ( $U_{Ni}=6$  eV). The calculated band gap values are marked in Fig. 3b and f, and d and h for pristine and Cu-substituted NiWO<sub>4</sub>, respectively. The charge density map on the (013) plane around the VBM ( $E_F-1$  eV to  $E_F$ ) for (i) NiWO<sub>4</sub> and (j) Ni<sub>0.875</sub>Cu<sub>0.125</sub>WO<sub>4</sub>. (k) Frequency dependent  $\varepsilon$  values measured by the impedance spectroscopy for Ni<sub>1-x</sub>Cu<sub>x</sub>WO<sub>4</sub> samples.

10 l

equation:18

**Materials Horizons** 

$$\alpha = e^2 \left( \frac{1}{\varepsilon_{\infty}} - \frac{1}{\varepsilon_0} \right) \sqrt{\frac{m}{2\omega_0}} \tag{1}$$

where  $\varepsilon_0$  and  $\varepsilon_\infty$  are the static and high-frequency dielectric constants, m is the effective mass, and  $\omega_0$  is the characteristic longitudinal optical phonon frequency. From eqn (1), enhancing  $\varepsilon$  inevitably reduces  $\alpha$ , thus it enlarges the polaron radius under long-range electron–phonon interactions, resulting in Fröhlich polaronic conduction. This result, combined with the discussion reported in Section S13 in the ESI, indicates that Cu substitution plays a critical role in  $\mu_{\rm H}$  enhancement by promoting the ionic polarizability in the system, while minimally influencing the electronic structure, since the correlation degree is preserved.

# Material feasibility test in QD-LED and oxide p/n junction rectifier devices

105

f(Hz)

104

Finally, we explored the use of p-type  $\mathrm{Ni}_{1-x}\mathrm{Cu}_x\mathrm{WO}_4$  as a HTL in opto-electronic devices. For QD-LED and p/n junction diode applications,  $\mathrm{Ni}_{1-x}\mathrm{Cu}_x\mathrm{WO}_4$  films of different thicknesses and functionality [30 nm as a conductive layer and 100 nm as a semiconducting layer (see Fig. S13, ESI†)] were fabricated by RF magnetron sputtering of a  $\mathrm{Ni}_{1-x}\mathrm{Cu}_x\mathrm{WO}_4$  target (x=0.185) with pure Ar and an  $\mathrm{Ar}/\mathrm{O}_2$  mixture ( $\mathrm{Ar}:\mathrm{O}_2=2:1$ ), respectively. Detailed film deposition conditions and device fabrication can be found in the Methods section. Fig. 4a and b show the Raman and UV-vis transmittance spectra, respectively, of conductive and semiconducting  $\mathrm{Ni}_{0.815}\mathrm{Cu}_{0.185}\mathrm{WO}_4$  films deposited on glass substrates. As shown in Fig. 4a, the characteristic W–O  $\mathrm{Ag}$  Raman peaks of sputtered samples are slightly blue-shifted and broadened (460, 560 and 960 cm<sup>-1</sup>, see the arrows in Fig. 4a) compared to those of the bulk samples (420, 550 and

Communication Materials Horizons

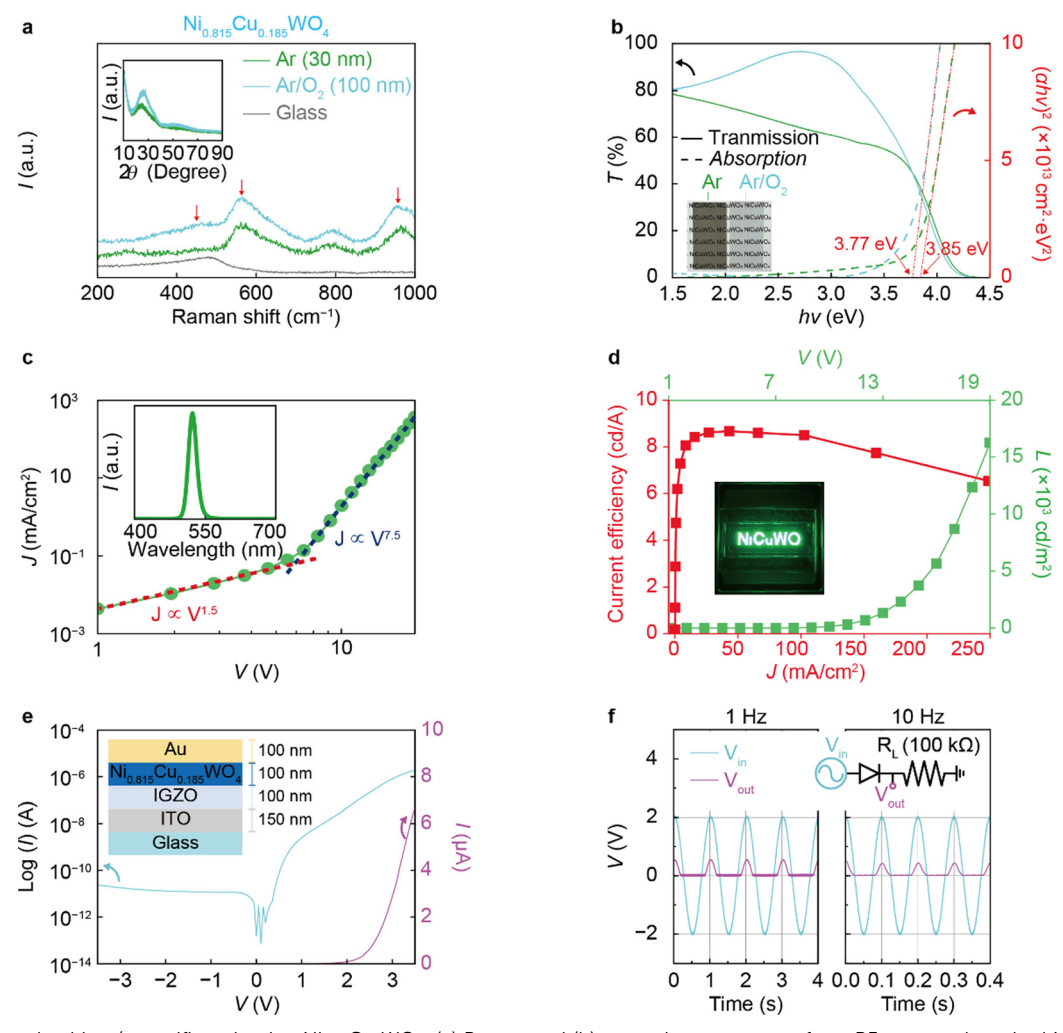


Fig. 4 QD-LED and oxide p/n rectifier adopting  $Ni_{1\_x}Cu_xWO_4$ . (a) Raman and (b) transmittance spectra from RF-sputter deposited  $Ni_{0.815}Cu_{0.185}WO_4$  thin films on glass substrate fabricated in Ar only (30 nm, for use in QD-LED) and Ar/O<sub>2</sub> (100 nm, for use in a rectifier diode) conditions. The XRD results and photo of the  $Ni_{0.815}Cu_{0.185}WO_4$  thin-film are displayed in the inset of Fig. 4a and b, respectively. (c) Current density (*J*) – voltage (*V*), (d) current efficiency (left axis) – *J*, and luminescence (*L* in right axis) – *V* curves of a QD-LED utilizing  $Ni_{0.815}Cu_{0.185}WO_4$  as the HTL. The electroluminescence (EL) spectrum and photograph of green emission are shown in the inset of Fig. 4c and d, respectively. (e) Current (*I*) – *V* characteristic of a p- $Ni_{0.815}Cu_{0.185}WO_4/n$ -IGZO junction diode. The oxide-based p/n diode schematic is illustrated in the inset of Fig. 4e. (f) AC to DC rectifying behaviour using a 2 V peak-to-peak sinusoidal input voltage ( $V_{in}$ ) and the corresponding output voltage ( $V_{out}$ ) signal. The circuitry configuration is schematically shown in the inset of Fig. 4f.

900 cm<sup>-1</sup>, Fig. S4, ESI†), due to the amorphous phase (see the inset XRD in Fig. 4a).<sup>28</sup> However, the direct  $E_{\rm g}$ 's of all samples are almost identical to those measured for the bulk (Fig. 4b), corroborating the quality of the sputtered thin-films and the reproducibility of Cu incorporation in NiWO<sub>4</sub>. The slight reduction in  $E_{\rm g}$  values in thin films are mainly attributed to the tail states formation originating from the amorphous nature.<sup>36,37</sup> The transmittance in the visible region for the most transparent film (100 nm thick, Ar/O<sub>2</sub> deposited) is ~96%, demonstrating its transparent nature as a p-type TCO film.

Fig. S14a (ESI $\dagger$ ) reports the schematic representation and the high-resolution cross-sectional transmission electron microscopy (HR-TEM) image of the QD-LED device with a 30 nm thick Ni<sub>0.815</sub>Cu<sub>0.185</sub>WO<sub>4</sub> HTL deposited under Ar-only working pressure conditions to enhance conductivity (refer to

Section S14 for discussion, ESI†). Note no additional blocking layers are used for balancing charge injection from the electrodes.  $^{38-43}$  The QD-LED energy band diagram in Fig. S14b (ESI†) indicates that the deep-lying VBM of Ni<sub>0.815</sub>Cu<sub>0.185</sub>WO<sub>4</sub> with a wide  $E_{\rm g}$  is beneficial not only for lowering the hole injection barrier, but also for increasing the electron-blocking barrier between the HTL and CdSe-based QD compared to other HTL materials.  $^{38-43}$  This advantage is reflected by the device performance. Fig. 4c shows the current density *versus* applied voltage (J–V) characteristics for the device, evidencing an ohmic conduction region ( $J \propto V^{1.5}$ ) up to 6.5 V and a clear trap-limited conduction region ( $J \propto V^{7.5}$ ) in the voltage regime higher than 6.5 V. Based on the ohmic conduction behaviour below 6.5 V, the Ni<sub>0.815</sub>Cu<sub>0.185</sub>WO<sub>4</sub> HTL serves as a simple charge conductor following Ohm's law.  $^{39,41}$  In the

**Materials Horizons** Communication

trap-limited conduction regime above 6.5 V, light emission occurs by electron-hole recombination in the QD layer acting as trap centres. 41,43 In the case of current-driven light-emitting diodes, the position of the electron-hole recombination zone is very important to prevent additional emission compromising colour purity.<sup>38,43</sup> Fig. 4c-inset shows only a single symmetric electroluminescence (EL) emission peak at 523 nm with a narrow full-width at half-maximum (FWHM) of 24.89 nm. demonstrating that balanced charge recombination only occurs in the QDs even without any additional blocking layers.38-43 Our QD-LED shows a maximum luminescence (L) and current efficiency ( $\eta$ ) of 16258 cd m<sup>-2</sup> and 8.67 cd A<sup>-1</sup>, respectively (Fig. 4d), which are greater than those of green CdSe QD devices with a similar structure (Table S4, ESI†). Since the roll-off behaviour of  $\eta$  is relatively small compared to other CdSe-based QD-LEDs, the significantly improvement device performance is attributed to enhanced hole-electron charge balance.<sup>38-43</sup>

Additionally, we broaden applicability of our p-type TCO to circuitry by fabricating an oxide-based p/n junction rectifier. As displayed in Fig. 4e-inset, a 100 nm-thick p-Ni<sub>0.815</sub>Cu<sub>0.185</sub>-WO<sub>4</sub> layer is deposited on an n-type IGZO film of the same thickness, resulting in a transparent oxide p/n junction. The I-V characteristic in Fig. 4e demonstrates prominent rectifying behaviour with a high on/off current ratio of 5.6  $\times$  10<sup>4</sup> compared to other oxide diodes (Table S5, ESI†). Considering that n-IGZO and p-Ni<sub>0.815</sub>Cu<sub>0.185</sub>WO<sub>4</sub> are both amorphous with an identical thickness, this good switching behaviour originates from their well-balanced charge transport characteristics under a large built-in potential (Fig. S15, ESI†). Next, taking advantage of the good diode characteristics, an AC to DC converting circuit is assembled with a 100 k $\Omega$  load resistor ( $R_{\rm L}$ ). As shown in Fig. 4f, when a sinusoidal input signal  $(V_{in})$  is applied with a −2 to +2 V peak-to-peak amplitude, AC to DC signal rectification can be measured up to 10 Hz without delaying. These results demonstrate the applicability of this new material for practical transparent device applications.

# Conclusions

We demonstrated the underlying physics of a new hole transparent conductor, Ni<sub>1-x</sub>Cu<sub>x</sub>WO<sub>4</sub>, with performance comparable to those from the other p-TCOs, while exhibiting the deepest  $\Phi$  value. Structural, compositional, and vibrational studies revealed that Cu substitutes Ni, resulting in Ni<sub>1-x</sub>Cu<sub>x</sub>WO<sub>4</sub> solid solutions up to x = 0.20. Electrical measurements confirm that the  $\mu_{\rm H}$  of NiWO<sub>4</sub> significantly increases by Cu incorporation, even leading to the emergence of band-like large polaronic conduction behaviour. The  $E_{\rm g}$ ,  $T_{\rm N}$ , and  $\Phi$  values of Ni<sub>1-x</sub>-Cu<sub>x</sub>WO<sub>4</sub> minimally change with the Cu content, supporting the sustained electron correlation strength in NiWO<sub>4</sub> regardless of the Cu content. DFT calculations and impedance spectroscopy measurements demonstrate that the enhanced polarizability plays a crucial role in the emergence of delocalized hole transport along a rigid deep-lying VBM band down to 5.77 eV. Finally, we utilized Ni<sub>1-x</sub>Cu<sub>x</sub>WO<sub>4</sub> films as the HTL and p-type layer in QD-LEDs and

rectifier devices, demonstrating the use of this p-type TCO in practical applications. Our results offer a novel strategy for expanding the functionality of strongly correlated materials and p-type TCO design.

# **Author contributions**

K. L., K. H. L., M. S. O., and A. F.: conceptualization, resources, supervision, validation, funding acquisition, project administration, writing - original draft, and writing - review & editing. S. Y. L., I. K., and H. J. K.: data curation, formal analysis, investigation, methodology, validation, and visualization. S. S., J. H. K., S. Y., J. B., K. W. P, C. J. H., H. M. K., H. Y., B. J. K., and S. I.: data curation, investigation, resources, software, and validation.

# Data availability

The data supporting this article have been included as part of the ESI.†

# Conflicts of interest

There are no conflicts to declare.

# Acknowledgements

This work was supported by the National Research Foundation of Korea (NRF) grant funded by the Korean government (MSIT) (No. RS-2024-00401881, No. 2022R1A2C2005210, and No. RS-2024-00411892). It was also financially supported by the Ministry of Trade, Industry and Energy (MOTIE) and Korea Planning & Evaluation Institute of Industrial Technology (KEIT) through the Industry Technology R&D Program (20016332). It was also supported by Samsung Research Funding & Incubation Center of Samsung Electronics under Project Number SRFC-MA1902-03. AF acknowledges NSF (award # 2223922) for support.

# References

- 1 S. M. Sze and K. K. Ng, Physics of Semiconductor Devices, John Wiley & Sons, 3rd edn, 2007.
- 2 S. M. Kang and Y. Leblebici, CMOS Digital Integrated Circuits: Analysis and Design, McGraw-Hill, 3rd edn, 2003.
- 3 K. Nomura, J. Inf. Disp., 2021, 22, 211.
- 4 A. M. Ionescu and H. Riel, Nature, 2011, 479, 329.
- 5 K. Fai and J. Shan, Nat. Photonics, 2016, 10, 216.
- 6 S. O. Kasap, Optoelectronics and Photonics: Principles and Practices, Pearson Education, 2nd edn, 2013.
- 7 A. Polman, M. Knight, E. C. Garnett, B. Ehrler and W. C. Sinke, Science, 2016, 352, aad4424.
- 8 X. Yu, T. J. Marks and A. Facchetti, Nat. Mater., 2016, **15**, 383.
- 9 D. S. Ginley, H. Hosono and D. C. Paine, Handbook of Transparent Conductors, Springer, 2010.
- 10 J. E. Medvedeva, D. B. Buchholz and R. P. H. Chang, Adv. Electon. Mater., 2017, 3, 1700082.

Communication **Materials Horizons** 

- 11 A. Murat, A. Adler, T. O. Mason and J. E. Medvedeva, J. Am. Chem. Soc., 2013, 135, 5685-5692.
- 12 B. Wang, et al., Nat. Commun., 2020, 11, 2405.
- 13 J. Kim, M. Jeong, B. Kim and J. Jang, IEEE Elec. Dev. Lett., 2022, 43, 1471.
- 14 Z. Wang, P. K. Navak, J. A. Caraveo-Frescas and H. N. Alshareef, Adv. Mater., 2016, 28, 3831.
- 15 M. T. Greiner, et al., Nat. Mater., 2012, 11, 76.
- 16 P. A. Cox, The Electronic Structure and Chemistry of Solids, Oxford University Press, 1987.
- 17 I. G. Austin and N. F. Mott, Adv. Phys., 2001, 50, 757.
- 18 C. Franchini, M. Reticcioli, M. Setvin and U. Diebold, Nat. Rev. Mater., 2021, 6, 560.
- 19 L. Zhang, et al., Nat. Mater., 2016, 15, 204.
- 20 K. H. L. Zhang, et al., Adv. Mater., 2015, 27, 5191.
- 21 S. G. Park, et al., Inorg. Chem. Front., 2020, 7, 853.
- 22 G. Kresse and D. Joubert, Phys. Rev. B: Condens. Matter Mater. Phys., 1999, 59, 1758.
- 23 G. Kresse and J. Furthmüller, Phys. Rev. B: Condens. Matter Mater. Phys., 1996, 54, 11169.
- 24 J. P. Perdew, K. Burke and M. Ernzerhof, Phys. Rev. Lett., 1996, 77, 3865.
- 25 S. L. Dudarev, G. A. Botton, S. Y. Savrasov, C. J. Humphreys and A. P. Sutton, Phys. Rev. B: Condens. Matter Mater. Phys., 1998, 57, 1505.
- 26 H. Eskes, L. H. Tjeng and G. A. Sawatzky, Phys. Rev. B: Condens. Matter Mater. Phys., 1990, 41, 288.

- 27 R. Tesch and P. M. Kowalski, *Phys. Rev. B*, 2022, **105**, 195153.
- 28 A. Kuzmin, J. Purans and R. Kalendarev, Ferroelectrics, 2001, 258, 21.
- 29 J. H. Ryu, et al., Scr. Mater., 2020, 182, 6.
- 30 C. C. Wang, S. A. Akbar, W. Chen and V. D. Patton, *J. Mater.* Sci., 1995, 30, 1627.
- 31 T. Sakanoue and H. Sirringhaus, Nat. Mater., 2010, 9, 736.
- 32 M. A. Pronsnikov, V. Y. Davydov, A. N. Smirnov, M. P. Volkov and R. V. Pisarev, Phys. Rev. B, 2017, 96, 014428.
- 33 M. Imada, A. Fujinori and Y. Tokura, Rev. Mod. Phys., 1998, **70**, 1039.
- 34 K. Lee, S. W. Kim, Y. Toda, S. Matsuishi and H. Hosono, Nature, 2013, 494, 336.
- 35 J. E. Medvedeva, V. I. Anisimov, O. N. Mryasov and A. J. Freeman, J. Phys.: Condens. Matter, 2022, 14, 4533.
- 36 T. Kamiya and H. Hosono, NPG Asia Mater., 2010, 2, 15.
- 37 T. Kamiya, K. Nomura and H. Hosono, Phys. Status Solidi A, 2009, 206, 860.
- 38 X. Yang, et al., Nano Energy, 2018, 46, 229.
- 39 Y. Jiang, et al., ACS Appl. Mater. Interfaces, 2019, 11, 11119.
- 40 Y. Zhang and L. Zhao, J. Mater. Res., 2019, 34, 2757.
- 41 J. M. Caruge, J. E. Halpert, V. Wood, V. Bulović and M. G. Bawendi, Nat. Photonics, 2008, 2, 247.
- 42 W. Ji, et al., ACS Photonics, 2017, 4, 1271.
- 43 H. Y. Kim, et al., Adv. Funct. Mater., 2016, 26, 3454; H. Eskes, L. H. Tjeng and G. A. Sawatzky, Phys. Rev. B: Condens. Matter Mater. Phys., 1990, 41, 288.